VOL. 23, NO. 2, 2024, 136-143
elektrika.utm.my
ISSN 0128-4428

ELEKTRIKA
Journal of Electrical Engineering

Diameter Optimization of No-Core Fiber for High Refractive Index Sensing

Nurul Farah Adilla Zaidi[1], **Nur Najahatul Huda Saris**[1*], **Muhammad Yusof Mohd Noor**[1], **Mohd Rashidi Salim**[1], **Sumiaty Ambran**[2]

[1]Faculty of Electrical Engineering, Universiti Teknologi Malaysia, 81310 Johor, Johor Bahru, Malaysia
[2]Malaysia-Japan International Institute of Technology, Universiti Teknologi Malaysia, 54100 Kuala Lumpur, Malaysia

[*]Corresponding author: nurnajahatulhuda@utm.my

Abstract: This study presents a simulation-based modal analysis to optimize the no-core fiber (NCF) sensor design for high refractive index (HRI) applications. The goal is to improve the sensitivity of the sensor towards HRI by solving problems in conventional optical fiber sensors (OFS), such as sophisticated fabrication methods, high fragility, and potential effects on long-term reliability. Furthermore, in previous work, most OFS applications focused on detecting mediums with a low refractive index (LRI). Hence, the goal of this study is to overcome these constraints. For this research, the Wave Optics module in COMSOL Multiphysics® software was used to optimize the NCF diameter, which ranged from 100 µm to 150 µm. Simulations include changes in the refractive index (RI) of the analyte in the surrounding medium of the sensor to analyse the efficiency of the NCF in HRI sensing completely, ranging from 1.46 RIU to 1.56 RIU. The performance is then assessed by monitoring the intensity change in the power spectrum, which reflects the reaction of leaky modes to various HRI conditions. The findings indicate that decreasing the size of the NCF sensor enhances sensitivity in detecting HRI mediums by amplifying the leakage loss of each order leaky mode, as opposed to a larger NCF diameter. This effect is due to the reduced confinement of modes in a smaller diameter NCF. The 100 µm diameter NCF has exceptional refractive index (RI) sensitivity and linearity, measuring 88.996 dB/RIU and 0.7783, respectively. Accordingly, NCF proves to be a promising candidate for utilization in HRI sensing applications, given its high sensitivity and straightforward fabrication, making it easily implementable and practical for real-world use.

Keywords: Diameter Optimization, No-core Fiber, Refractive Index, Sensor, Simulation

Article History: received 10 March 2024; accepted 7 August 2024; published 29 August 2024

1. INTRODUCTION

The utilization of optical fiber sensors (OFS) for refractive index (RI) sensing has gained prominence due to their attributes, such as high sensitivity [1,2], rapid response [3,4], lightweight [5,6], compact size [7,8], multiplexing capabilities [9,10], chemical inertness [11,12], and resistance to electromagnetic interference (EMI) [13,14]. Despite the existence of various proposed RI fiber sensor designs, such as surface plasmon resonance [15,16], interferometers [17,18], gratings [19, 20], and multimode interference [21, 22], challenges persist, including complex fabrication processes [23,24], high fragility [25,26], and a predominant focus on detecting substances with lower RI [27,28].

While some literature demonstrates OFS performance for HRI sensors, some limitations remain, as mentioned earlier [29,30]. For instance, in 2016, tin-dioxide thin films were utilised in optical fiber interferometers for oil sensing. During the study, several challenges arose concerning coating thickness variations that affect long-term reliability and sensitivity to temperature [31]. In 2017, Mahanta et al. proposed an etched polymer fiber with higher RI than the oil, achieving high sensitivity at 194.41 dBm. However, complex fabrication and sensitivity to surrounding temperature were observed due to the polymer material's high thermo-optic coefficient (TOC) [32]. In 2019, etched MMF demonstrated high sensitivity up to 972.18 dBm, but its fragile structure and challenges in implementation were attributed to chemical etching's side effects and cross-sensitivity to temperature [32]. To address these issues, this research explores the use of no-core fiber (NCF) as a promising alternative. With a coreless design that directly exposes it to the surrounding medium, it enhances sensitivity toward high refractive index (RI) mediums, generating a knowledge gap and offering an alternative method for evaluating RI changes [33].

Previously, the NCF has been implemented to detect a lower RI surrounding medium, but limited studies have been conducted on higher RI, especially for assessing oil degradation [34-36]. In addition, different operation theories will be implemented for varying conditions of the RI of the surrounding medium. When the surrounding RI is lower than the NCF, the sensor operates based on guided modal interference (GMI) [37]. However, if the surrounding RI exceeds that of the NCF, it operates based on leaky modal interference (LMI), supporting a continuous spectrum of radiation modes [38]. As a result,

in this investigation that focuses on higher RI analyte detection, leaky modal interference (LMI) analysis is implemented. Nevertheless, some of the light leaks out during the assessment due to the higher RI medium surrounding the fiber.

In addition, most recent publications have primarily focused on experimental investigations and neglected the numerical analyses for performance comparisons of OFS structures for high-RI sensing [39,40]. Therefore, this research conducts a preliminary comparative performance analysis for NCF with different head diameters, ranging from 100 μm to 150 μm. The chosen diameter ranges of NCF provide high coupling efficiency and reliability with 125 μm single-mode fiber (SMF), which ensures reliability in future work. Apart from that, the implementation of NCF in this research is inspired by a similar theoretical idea for detecting high-RI sensing using a silica rod, as reported by Saimon et al. [41]. This approach eliminates the need for a cladding etching process.

Despite achieving a high sensitivity of 115.12 dBm/RIU in experimental work, practical experiments faced challenges due to the smaller size of the sensor head used at that time, which was 60 μm in diameter when coupled with an SMF of size 125 μm, which acted as the light carrier. Therefore, this simulation is conducted based on the suggested NCF size in a mode analysis study, considering analyte refractive index (RI) variations from 1.46 RIU to 1.56 RIU. These values represent the typical high-RI range of oil [39,42]. The performance is evaluated by observing the attenuation of the intensity spectrum due to the leaky mode interference factor (LMI) [43].

Accordingly, this research aims to address the need for a robust structural fiber without requiring cladding layer removal. This is commonly done with SMF and MMF in previous works, both of which possess a fragile fiber structure. Furthermore, this work highlights a significant knowledge gap in the diameter optimisation of NCF and its capability to sense a broad range of high-RI mediums, especially for potential applications in oil assessment based on leaky mode sensing theory.

2. SIMULATION PROCEDURE

In this research, simulation-based analysis was conducted using COMSOL Multiphysics 5.6® software with finite element analysis (FEA). The optimisation focused on various NCF diameters exposed to a high-RI analyte medium. Two-dimensional (2D) wave optics were employed for the simulation due to its advantages in simple meshing, low computer memory requirements, and short simulation time [44]. The analysis applied Maxwell's equations to examine electric field interactions in different media [45], ensuring the functionality of the sensor in high-RI conditions.

2.1 Sensor Design

The NCF diameter structures under investigation are illustrated in Figure 1. The diameter was optimised within the range of 100 μm to 150 μm to assess the sensitivity of the sensor toward HRI. This is achieved by observing the intensity change of the power spectrum resulting from the reaction of leaky modes for each diameter of NCF.

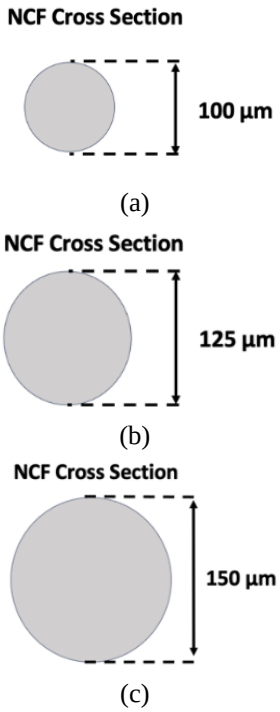

Figure 1. NCF sensor diameter in cross-section view at (a) 100 μm, (b) 125 μm, (c) 150 μm

2.2 Simulation Method and Workflow

The software offers two simulation study methods: mode analysis and boundary-mode analysis. Mode analysis allows users to study light within a specific frequency or wavelength domain through the NCF cross-section, providing insights into colored electric field intensity and mode field diameter (MFD) [46]. On the other hand, boundary-mode analysis is used to examine light propagation within the beam envelope through the longitudinal NCF structure, enabling the observation of MMI interference and electric field distribution along a horizontal line of the sensor structure [47]. Even though both mode and boundary-mode analyses have different functionalities, both share similar simulation workflows, as shown in Figure 2.

For this research, we will focus on the mode analysis of NCF. The primary objective is to observe the effect of diameter on the peak power (light behavior) at a specific cross-section when exposed to higher RI during the optimization of the sensor head diameter. In contrast, boundary analysis, which involves optimizing the length of the NCF to observe the overall signal peak at the output, will be included in future work.

The simulation begins with the creation of the geometry, incorporating the precise dimensions of the sensor. Each geometry is referred to as a domain that represents a distinct study area. Subsequently, it is required to allocate an RI for each domain material. Following this, the model undergoes meshing to break down the domain into smaller elements. Finally, all computations were performed to derive the results. If the solution encounters an error or an unsatisfactory computation, the simulation necessitates repetition. Conversely, if there are no issues, the results can be utilized for postprocessing.

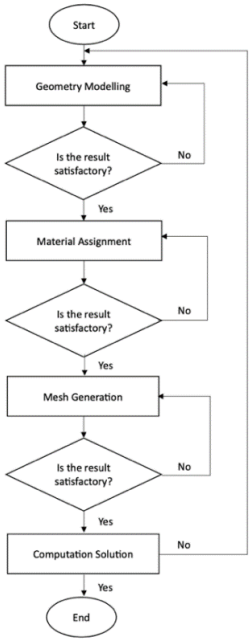

Figure 2. Simulation workflow for mode analysis and boundary mode analysis

2.2.1 Geometry Modelling and Material Assignment

Figures 3 (a), (b), and (c) illustrate the mode analysis geometry, which includes NCF and analyte domains in a cross-section view. The geometry is designed on a plane, with NCF diameter sizes of 100 µm, 125 µm, and 150 µm at the center. Each of them is surrounded by the analyte domain with a diameter of 200 µm in high refractive index (RI) conditions, ranging from analyte values of 1.46 RIU to 1.56 RIU, to assess the sensitivity of various NCF diameters. To reduce unwanted reflections at the computational boundaries, a perfectly matched layer (PML) is added to simulate a non-reflective infinite region. The PML is configured to adhere to the thickness recommended by the COMSOL, which is 4 µm. The specific geometric dimensions are summarised in Table 1.

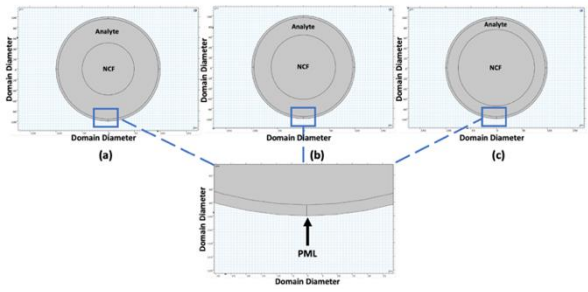

Figure 3. The geometry of the NCF (a) 100 µm, (b) 125 µm, and (c) 150 µm

Table 1. The domain dimension in the mode analysis

Domain Dimension	Value (µm)
NCF Diameter	100/ 125 / 150
Analyte Diameter	200
PML thickness	4

In determining the NCF RI (n_{NCF}), the Sellmeier equation is used and can be expressed in the following Equation (1) [48]:

$$n_{NCF}(\lambda) = \sqrt{1 + \frac{A_1\lambda^2}{\lambda^2-\lambda_1^2} + \frac{A_2\lambda^2}{\lambda^2-\lambda_2^2} + \frac{A_3\lambda^2}{\lambda^2-\lambda_3^2}} \quad (1)$$

From the Equation (1), n is the NCF RI, λ is the operating wavelength. The coefficient A_1, A_2 and A_3 can be obtained from the manufacturer of Flexilicate Sdn. Bhd, Malaysia. The calculation of NCF RI with the Sellmeier coefficient is summarised in Table 2.

Table 2. Sellmeier coefficient and NCF RI at 1550 nm operating wavelength

Sellmeier Coefficient					
A_1	A_2	A_3	λ_1	λ_2	λ_3
0.4873 60229	0.6175 09393	0.8771 51493	0.0028 14182	0.011 99919	96.33 26333
NCF RI (λ=1550 nm)					
1.4443 RIU					

In determining the analyte RI (n_a), the analyte used for RI measurement was a colourless liquid determined by the Cargille Laboratories, Series A, at an operating wavelength of 589.3 nm. Hence, the Cauchy equation is used to determine the exact RI of the analyte used for future experimental work with different operating wavelength values, as shown in Equation (2) [49]. A new RI should be calculated using the Equation below to simulate the exact readings of analyte RI for future use. From the Equation (2), n_a represent the RI of the analyte, and λ is the operating wavelength, which, for this research, is 1550 nm. The coefficients A, B and C can be obtained from the manufacturer datasheet. Different RI analytes have specific coefficients, as stated in the datasheet and summarised in Table 3.

$$n_a(\lambda) = A + \frac{B}{\lambda^2} + \frac{C}{\lambda^4} \quad (2)$$

Table 3. Cauchy coefficient and analyte RI at the operating wavelength

Manufacturer Analyte RI (λ = 589.3 nm) (RIU)	**Cauchy Coefficient**			**Real Analyte RI (λ = 1550 nm) (RIU)**
	A	**B**	**C**	
1.46	1.447925	4.0734	4.1636939	1.45
1.47	1.456781	4.4023	6.5427334	1.459
1.48	1.465636	4.7312	8.9217730	1.468
1.49	1.474492	5.0602	1.1300812	1.477

1.50	1.483347	5.3891	1.3679852	1.486
1.51	1.492203	5.7180	1.6058892	1.495
1.52	1.501058	6.0470	1.8437931	1.504
1.53	1.509914	6.3759	2.0816971	1.513
1.54	1.518770	6.7048	2.3196010	1.522
1.55	1.527625	7.0338	2.5575050	1.531
1.56	1.536481	7.3627	2.7954089	1.540

Subsequently, the simulation settings used are summarised in Table 4. The sensing medium RI is set from 1.46 RIU to 1.56 RIU, the typical range of a liquid RI used for OFS calibration for high-RI applications like oil sensing. All the RI mediums are set to isotropic. 1550 nm was chosen as the operating wavelength where the lowest attenuation window of practical fiber is established [50].

Table 4. Simulation settings

Parameter	Expression/ Setting	Value
Operating wavelength	-	1550 nm
NCF refractive index	Sellmeier equation	1.4443 RIU
Liquid refractive index	-	1.46 - 1.56 (Step: 0.01 RIU)
Refractive index medium	Isotropic	-

2.2.2 Mesh Generation and Computation Solution

Next, to satisfy mode propagation in the NCF region, the mesh generation for the mode analysis is shown in Figure 4. A free triangular element shape was used to generate the mesh of the circular domain. Each diameter size of the NCF domain was meshed with extremely fine element sizes to ensure high-quality sensor structure outputs. In contrast, the analyte domain was meshed with normal element sizes.

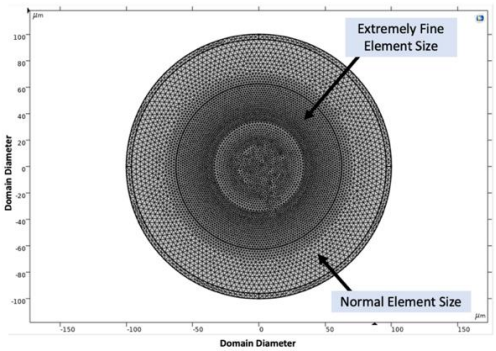

Figure 4. Mesh generation of NCF

The simulation studied the light in linearly polarized lowest order mode, LP_{01}. As the COMSOL study the model in the frequency domain, the relationship between frequency, f and operating wavelength, λ is considered to compute the solution at the selected operating wavelength, which can be expressed in Equation (3) [51]:

$$f = \frac{c}{\lambda} \tag{3}$$

Here, c is the speed of light. At a fixed c of 299792458 ms^{-1} (from COMSOL) and λ of 1550 nm, the f is found to be 193414.489 GHz.

Next, a cut line method is used to plot the dataset along the line, as shown in Figure 5. This step was important to visualize the dataset in the form of graphs, such as MFD, vertical or horizontal normalized electric field intensity. This method can be done by selecting the start and end points to form the line across the NCF cross-section. After settings have been configured, clicking the compute selection executes the simulation. The results are discussed in the Results and Discussion section.

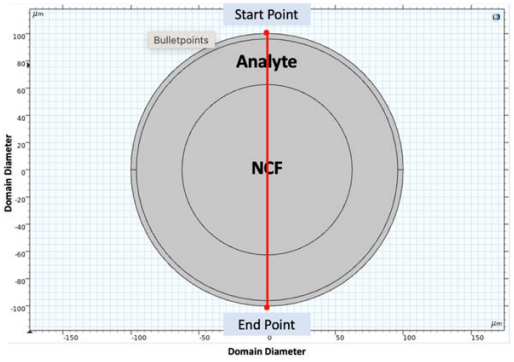

Figure 5. Cutline method in mode analysis for NCF

For assessing the sensor performance, the sensitivity of each NCF diameter can be defined as the change in input required to produce a unit change in output [52]. The sensitivity, S, can be expressed in Equation (4) [53]:

$$S = \frac{\Delta\lambda_{dip/peak}}{\Delta n_{analyte}} \tag{4}$$

Here, $\Delta\lambda_{dip/peak}$ is the change in dip/peak wavelength and $\Delta n_{analyte}$ is the change in analyte RI. The sensitivity unit is expressed in nm/RIU or dB/RIU [53]. The dip typically chosen to measure the sensitivity of the sensor is the one that is dominant and provides consistent and sensitive responses to changes in the measured parameter.

3. RESULTS AND DISCUSSION

During the simulation evaluation of the optimized NCF diameter sensor that measures different high RI analytes, varied colors in electric field intensity behavior and changes in MFD were exhibited for each NCF diameter. Based on the reduction observed in MFD, it can be concluded that a portion of light leaks out due to the RI mismatch between the NCF and the analyte boundary. Specifically, this study focuses on the peak power at the center of a particular cross-section, indicating observation of the signal at the center of the fiber. In this scenario, as the RI increases, light leaks out to the surrounding medium at that cross-section, resulting in a decrease in power signal. This phenomenon is attributed to the implementation of Fresnel reflection that causes some of the light to leak out due to the higher RI of the surrounding

medium compared to the RI of the NCF. The transition from red to blue in the colored electric field intensity indicates the attenuation of light energy when reaching boundaries with different RI mediums. The process involved capturing the peak points of the Electric Field Norm (V/m) for each RI scenario directly from the simulation result. Subsequently, these Electric Field Norm values were converted into optical power (dB) to facilitate direct comparison with prior studies and standardize our measurements. No specialized equipment beyond standard optical measurement tools was required for this data collection. The optical power values were derived from the Electric Field Norm measurements, ensuring accuracy and consistency in our analysis.

Figure 6, Figure 7, and Figure 8 show the colored electric field intensity and the MFD plot for the three different NCF fiber diameters, which were 100 µm, 125 µm, and 150 µm, respectively when exposed to HRI value of 1.46 RIU to 1.56 RIU. The intensity response changes for each diameter are observable, with 100 µm, the smaller diameter NCF sensors exhibiting more pronounced changes in intensity when exposed to high-RI surrounding medium compared to their larger counterparts due to a phenomenon known as mode confinement.

In optical fibers, various modes of light propagation are supported. Smaller diameter fibers primarily support the fundamental mode (LP_{01}), confining light to a smaller core area. This confinement leads to higher power density within the core, which enhances the responsiveness of the sensor to changes in the surrounding medium's refractive index. Additionally, due to the increased leakage loss of each-order leaky mode in smaller diameter NCF, this effect is attributed to the weaker confinement of modes. In contrast, the larger diameter fibers (150 µm) can support multiple modes, leading to lower sensitivity to changes in the medium's properties. For sensitivity characterisation, if the sensitivity of the sensors falls within the regression value range of 0.5 to 1 in the refractive indices, it will be deemed as good performance for sensing applications.

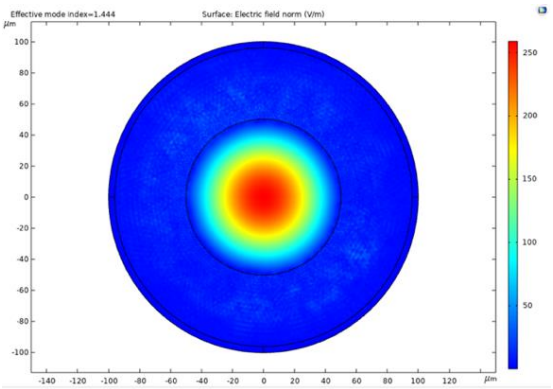

(a)

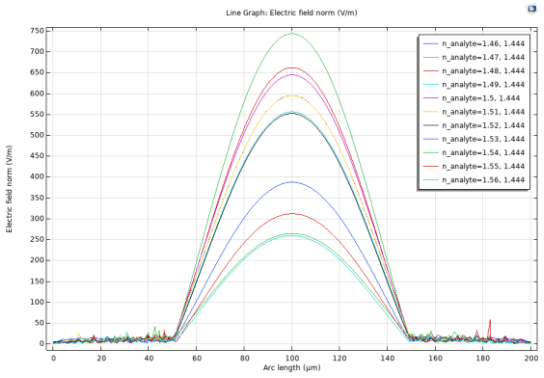

(b)

Figure 6. Mode analysis of the 100 µm NCF sensor when exposed to high-RI analyte presented in (a) coloured electric field intensity (b) MFD

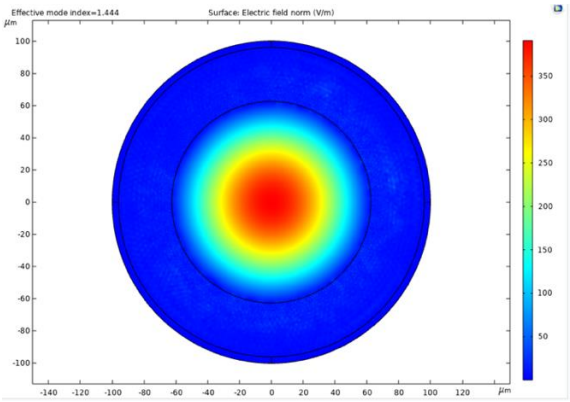

(a)

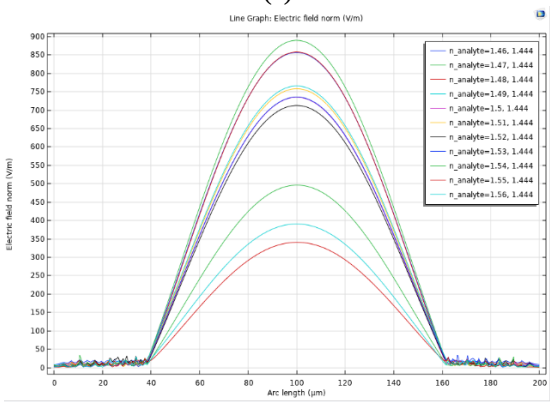

(b)

Figure 7. Mode analysis of the 125 µm NCF sensor when exposed to high-RI analyte presented in (a) coloured electric field intensity (b) MFD

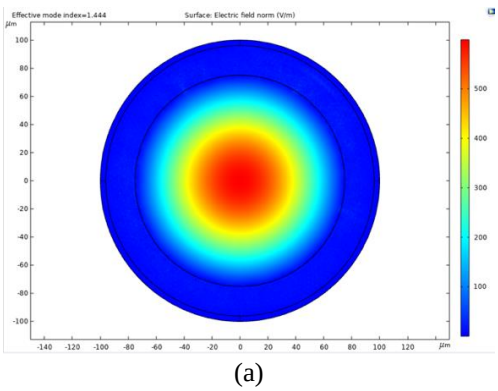

(a)

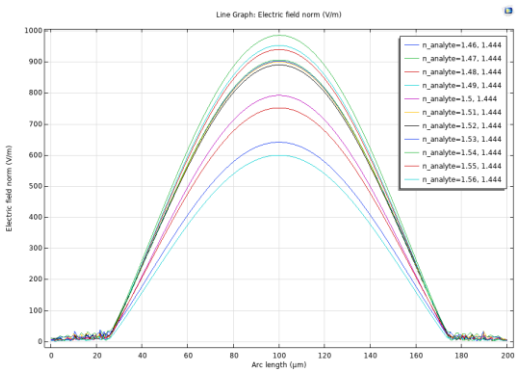

(b)

Figure 8. Mode analysis of the 150 μm NCF sensor when exposed to high-RI analyte presented in (a) coloured electric field intensity (b) MFD

Subsequently, the sensitivity results for each fiber diameter are depicted in Figure 9. The sensitivity of the sensor can be directly obtained from the graph slope. For the NCF with a diameter of 100 μm, the sensitivity was recorded to be 88.996 dB/RIU, corresponding to a linear regression value of 0.7783. On the other hand, the NCF with a diameter of 125 μm has a sensitivity of 75.136 dB/RIU with a linear regression value of 0.756, while the NCF with a diameter of 150 μm has a sensitivity of 30.86 dB/RIU with a linear regression value of 0.5069.

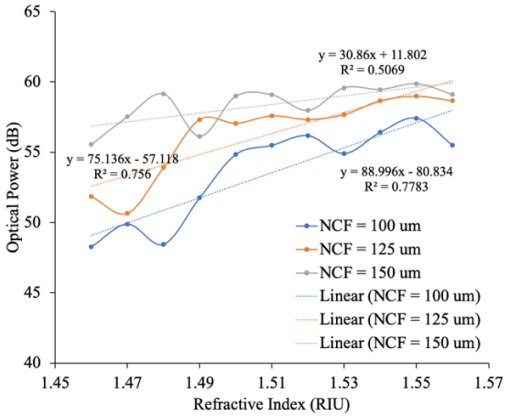

Figure 9. Sensitivity analysis for each NCF diameter

The result of the NCF optimisation is summarised in Table 5. Notably, the smallest diameter of NCF, which is 100 μm, exhibited the highest sensitivity of 88.996 dB/RIU compared to the other diameters. In fact, it is 2.8 times higher than that of 150 μm NCF diameter. Furthermore, the 100 μm sensor demonstrated high linearity, reaching up to 78%, indicating a good fit with the straight line. Hence, these findings demonstrate that smaller diameters yield higher sensitivity due to their capacity to concentrate optical power within a reduced core area, enabling more profound interactions with the high-RI surrounding medium. This aligns with theoretical expectations, as smaller diameters enhance the ability of the sensor to detect subtle changes in the surrounding environment. According to the literature, a smaller diameter leads to a more complex fabrication method [29, 41] Additionally, it compromises the mechanical strength of the fiber and complicates handling for experimental purposes. Therefore, in this work, the diameter is limited to 100 μm.

Table 5. The summary of the optimisation results for NCFs.

Diameter	Sensitivity (dB/RIU)	Regression
100 μm	88.996	0.7783
125 μm	75.136	0.756
150 μm	30.86	0.5069

Table 6 compares the performance of previously studied optical fiber-based RI sensors in terms of sensor structure, RI range, sensor head diameter, and sensitivity. References [54-57] indicate that all these sensors require complex fabrication processes involving polished, etched, or tapered structures, which make them more fragile and susceptible to breakage. Moreover, these sensors are only capable of detecting RI values lower than the fiber's RI, based on wavelength shift responses. In contrast, the sensor referenced in [29] can detect RI values higher than the fiber's RI with a sensitivity of 76.63 dB/RIU, although it also requires an etched structure. These sensor designs depend on reduced diameter fiber structures to enhance sensitivity.

Next, a notable development in 2022 involved the introduction of a silica rod-based high RI (HRI) sensor. The best sensitivity achieved by this silica rod in theoretical simulations was 248.95 dB/RIU with a sensor head diameter of 50 μm. However, the lowest sensitivity for the silica rod sensor was 80.14 dB/RIU with a head diameter of 100 μm. Despite its high sensitivity, the silica rod structure with smallest size is inherently fragile, making it difficult to splice and cleave for experimental purposes. Consequently, the researchers opted for a larger sensor head size to prevent easy breakage [41].

In contrast, the sensor proposed in this study achieves high sensitivity by reducing the no-core fiber (NCF) sensor head diameter to 100 μm without compromising structural integrity. The coreless characteristic of the NCF allows for direct use as a sensor without the need for complex fabrication processes, thereby enhancing sensitivity and sensor. Additionally, optimization studies have been conducted to evaluate sensor head diameters both slightly below and slightly above the standard 125 μm head diameter, ensuring the structural strength of the fiber for future experimental purposes.

Table 6. The performance comparison of the optical fiber-based RI sensors

Structure	RI range (RIU)	SHD (μm)	Sensitivity (/RIU)	Fabrication complexity
Double-polished	1.345-1.405	65	151.29 nm	Required chemical

MMF [54]				
Side-polished MMF [55]	1.43-1.45	104.73	1190 nm	Needs an additional experimental setup to polish the fiber
Etched NCF [56]	1.32-1.35	25	1442 nm	Required acidic chemical
Tapered NCF [57]	1.333-1.350	13	686 nm	Needs an additional experimental setup and specialized tools to taper the fiber
Etched MMF [29]	1.46-1.55	105	76.63 dB	Required acidic chemical
Silica Rod [41]	1.45-1.531	50 & 100	248.95 dB & 80.14 dB	Customize the splicing procedure to accommodate the very small diameter of the fiber.
Our Work	1.46–1.56	100	88.996 dB	Standard splicing process

4. CONCLUSION

This paper demonstrates the performance of NCF design with different diameters at various high-RI analytes, ranging from 1.46 RIU to 1.56 RIU. The design has been successfully simulated using COMSOL software to determine sensor characteristics toward high-RI. Optimizing various NCF diameters is essential for discovering the most effective design that enhances sensitivity in high RI conditions and simplifies the fabrication process. In this work, NCF with a diameter of 100 μm achieves the highest sensitivity at 88.996 dB/RIU, corresponding to a linear regression value of 0.7783. This can be attributed to the lower confinement modes in a smaller diameter NCF. Therefore, this characteristic establishes NCF as a robust and excellent fiber sensor for high-RI sensing applications, as it is directly exposed to the surrounding medium. Hence, NCF demonstrates significant potential in sensing applications for high-RI variations, especially for oil degradation assessment. It is simple to put into practice and has the potential to be driven towards industrialized mass production, making it an ideal tool for deployment.

ACKNOWLEDGMENT

This work was supported by Ministry of Education Malaysia under the Fundamental Research Grant Scheme (FRGS/1/2023/TK07/UTM/02/19) and UTM Fundamental Research (UTMFR) vot grant number Q.J130000.3851.21H76.

REFERENCES

[1] Zhao, Y., J. Zhao, and Q. Zhao, *Review of no-core optical fiber sensor and applications.* Sensors and Actuators A: Physical, 2020. **313**: p. 112160.

[2] Zhao, Y., J. Zhao, and Q. Zhao, *High sensitivity seawater temperature sensor based on no-core optical fiber.* Optical Fiber Technology, 2020. **54**: p. 102115.

[3] Roriz, P., et al., *Optical fiber temperature sensors and their biomedical applications.* Sensors, 2020. **20**(7): p. 2113.

[4] Sahota, J.K., N. Gupta, and D. Dhawan, *Fiber Bragg grating sensors for monitoring of physical parameters: A comprehensive review.* Optical Engineering, 2020. **59**(6): p. 060901-060901.

[5] Min, R., et al., *Optical fiber sensing for marine environment and marine structural health monitoring: A review.* Optics & Laser Technology, 2021. **140**: p. 107082.

[6] Wu, T., et al., *Recent progress of fiber-optic sensors for the structural health monitoring of civil infrastructure.* Sensors, 2020. **20**(16): p. 4517.

[7] Floris, I., et al., *Fiber optic shape sensors: A comprehensive review.* Optics and Lasers in Engineering, 2021. **139**: p. 106508.

[8] Du, C., et al., *A review of railway infrastructure monitoring using fiber optic sensors.* Sensors and Actuators A: Physical, 2020. **303**: p. 111728.

[9] Leal-Junior, A.G., et al., *Multiplexing technique for quasi-distributed sensors arrays in polymer optical fiber intensity variation-based sensors.* Optics & Laser Technology, 2019. **111**: p. 81-88.

[10] Zhu, C., R.E. Gerald, and J. Huang, *Progress toward sapphire optical fiber sensors for high-temperature applications.* IEEE Transactions on Instrumentation and measurement, 2020. **69**(11): p. 8639-8655.

[11] Wang, R., et al., *Stretchable gold fiber-based wearable textile electrochemical biosensor for lactate monitoring in sweat.* Talanta, 2021. **222**: p. 121484.

[12] Gong, P., et al., *Optical fiber sensors for glucose concentration measurement: A review.* Optics & Laser Technology, 2021. **139**: p. 106981.

[13] Diaz, C.A., et al., *Optical fiber sensing for sub-millimeter liquid-level monitoring: A review.* IEEE sensors journal, 2019. **19**(17): p. 7179-7191.

[14] He, R., et al., *Polymer optical fiber liquid level sensor: A review.* IEEE Sensors Journal, 2021. **22**(2): p. 1081-1091.

[15] Zhao, Y., et al., *Current status of optical fiber biosensor based on surface plasmon resonance.* Biosensors and Bioelectronics, 2019. **142**: p. 111505.

[16] Gandhi, M.A., et al., *Recent advances in plasmonic sensor-based fiber optic probes for biological applications.* Applied Sciences, 2019. **9**(5): p. 949.

[17] Miliou, A. *In-fiber interferometric-based sensors: Overview and recent advances*. in *Photonics*. 2021. MDPI.

[18] Bhardwaj, V., K. Kishor, and A.C. Sharma, *Tapered optical fiber geometries and sensing applications based on Mach-Zehnder Interferometer: A review.* Optical Fiber Technology, 2020. **58**: p. 102302.

[19] Warren-Smith, S.C., et al., *Stability of grating-based optical fiber sensors at high temperature.* IEEE Sensors Journal, 2019. **19**(8): p. 2978-2983.
[20] Khan, F., et al., *Multi-core optical fibers with Bragg gratings as shape sensor for flexible medical instruments.* IEEE sensors journal, 2019. **19**(14): p. 5878-5884.
[21] Wu, Q., et al., *Singlemode-multimode-singlemode fiber structures for sensing applications—A review.* IEEE Sensors Journal, 2020. **21**(11): p. 12734-12751.
[22] Noor, S., et al. *Multimode interference based fiber-optic sensor for temperature measurement*. in *Journal of Physics: Conference Series*. 2019. IOP Publishing.
[23] Bag, S.K., et al., *Design and characterisation of surface relief grating on etched multimode optical fiber for refractive index sensing.* Sensors and Actuators A: Physical, 2020. **303**: p. 111836.
[24] Mohammed, H.A., *A taper-in-etch based hybrid fiber Mach-Zehnder interferometer hydrogen sensor*. Optical Fiber Technology, 2023. **80**: p. 103390.
[25] Jali, M.H., et al. *Optical Microfiber Sensor: A Review*. in *Journal of Physics: Conference Series*. 2021. IOP Publishing.
[26] Dai, M., et al., *State-of-the-art optical microfiber coupler sensors for physical and biochemical sensing applications.* Biosensors, 2020. **10**(11): p. 179.
[27] Qiu, S., et al., *Hollow-core negative curvature fiber with high birefringence for low refractive index sensing based on surface plasmon resonance effect.* Sensors, 2020. **20**(22): p. 6539.
[28] Wang, F., et al., *Folded-tapered multimode-no-core fiber sensor for simultaneous measurement of refractive index and temperature.* Optics & Laser Technology, 2020. **130**: p. 106333.
[29] Yang, L., et al., *Guided-mode-leaky-mode-guided-mode fiber structure and its application to high refractive index sensing.* Optics letters, 2012. **37**(4): p. 587-589.
[30] Xue, L.-L., D. Che, and L. Yang, *High refractive index sensing based on single leaky mode attenuation.* Optics Communications, 2013. **294**: p. 198-201.
[31] Zubiate, P., et al., *Fabrication of optical fiber sensors for measuring ageing transformer oil in wavelength.* IEEE Sensors Journal, 2016. **16**(12): p. 4798-4802.
[32] Mahanta, D.K. and S. Laskar, *Investigation of transformer oil breakdown using optical fiber as sensor*. IEEE Transactions on Dielectrics and Electrical Insulation, 2018. **25**(1): p. 316-320.
[33] Wang, K., et al., *Advances in optical fiber sensors based on multimode interference (MMI): a review.* IEEE Sensors Journal, 2020. **21**(1): p. 132-142.
[34] Chen, Y., et al., *Wavelength dependence of the sensitivity of all-fiber refractometers based on the singlemode–multimode–singlemode structure.* IEEE Photonics Journal, 2014. **6**(4): p. 1-7.
[35] Li, Y., Z. Liu, and S. Jian, *Multimode interference refractive index sensor based on coreless fiber.* Photonic Sensors, 2014. **4**: p. 21-27.
[36] Xu, S., et al., *Optimization Design of SNS Sensor Structural Parameters for Battery Expansion Monitoring.* Frontiers in Energy Research, 2021. **9**: p. 725458.
[37] Soldano, L.B. and E.C. Pennings, *Optical multimode interference devices based on self-imaging: principles and applications.* Journal of lightwave technology, 1995. **13**(4): p. 615-627.
[38] Wang, P., et al., Optics letters, 2011. **36**(12): p. 2233-2235.
[39] Razzaq, A., et al., *Measurement of ester-based transformer oil aging using tapered single mode-multimode-single mode fiber structure.* Microwave and Optical Technology Letters, 2020. **62**(2): p. 559-564.
[40] Hayber, Ş.E., T.E. Tabaru, and M. Güçyetmez, *Evanescent field absorption-based fiber optic sensor for detecting power transformer oil degradation.* Fiber and Integrated Optics, 2021. **40**(4-6): p. 229-248.
[41] Saimon, S.M., et al., *Single-Mode-Multimode Silica Rod-Single-Mode High Refractive Index Fiber Sensor.* IEEE Sensors Journal, 2022. **22**(11): p. 10559-10566.
[42] Razzaq, A., et al., *Measurement of dissolved decay products of transformer oil using D-shaped plastic optical fiber as a sensor.* IET Science, Measurement & Technology, 2020. **14**(10): p. 901-905.
[43] Saimon, S.M., et al., *A high sensitivity refractive index sensor based on leaky mode coupler of MMI.* IEEE Photonics Technology Letters, 2021. **34**(1): p. 63-66.
[44] McCoy, D.E., et al., *Finite-difference time-domain (FDTD) optical simulations: a primer for the life sciences and bio-inspired engineering.* Micron, 2021. **151**: p. 103160.
[45] Jin, J.-M., *Theory and computation of electromagnetic fields*. 2015: John Wiley & Sons.
[46] Chen, Y., et al., *Side-polished single-mode-multimode-single-mode fiber structure for the vector magnetic field sensing.* Journal of Lightwave Technology, 2020. **38**(20): p. 5837-5843.
[47] Younus, S.I., A.A. Al-Dergazly, and A. Abass. *Characterisation of Multimode Interference Based Optical Fiber*. in *IOP Conference Series: Materials Science and Engineering*. 2021. IOP Publishing.
[48] Khanikar, T. and V.K. Singh, *Gold grating assisted SPR based D-shaped single mode fiber for detection of liquid refractive index.* Optical and Quantum Electronics, 2019. **51**: p. 1-10.
[49] Nkoma, J.S. and P.K. Jain, *Introduction to Optics: Geometrical, Physical and Quantum*. 2019: Mkuki na Nyota Publishers.
[50] Holmes, C., et al., *Evanescent field refractometry in planar optical fiber.* Optics letters, 2018. **43**(4): p. 791-794.
[51] Han, X., et al., *Influence of coupling conditions on the time delay characteristics of parallel-cascaded optical waveguide ring resonators.* Optik, 2013. **124**(5): p. 377-384.
[52] McGrath, M.J., et al., *Sensing and sensor fundamentals.* Sensor technologies: Healthcare, wellness, and environmental applications, 2013: p. 15-50.
[53] Xiao, G., et al. *Graphene oxide sensitised no-core fiber step-index distribution sucrose sensor*. in *Photonics*. 2020. MDPI.